Electronic Supplementary Material (ESI) for Sustainable Energy & Fuels.

Supporting Information

Binder-free Mn-V-Sn oxyhydroxide decorated with metallic Sn as earth-abundant supercapattery electrode for intensified energy storage

Loujain G. Ghanem ǂ, Manar M. Taha ǂ, Mohamed Salama, Nageh K. Allam *

Energy Materials Laboratory (EML), School of Sciences and Engineering, The American University in Cairo, New Cairo, 11835, Egypt

* Corresponding Author: nageh.allam@aucegypt.edu (N. K. Allam)

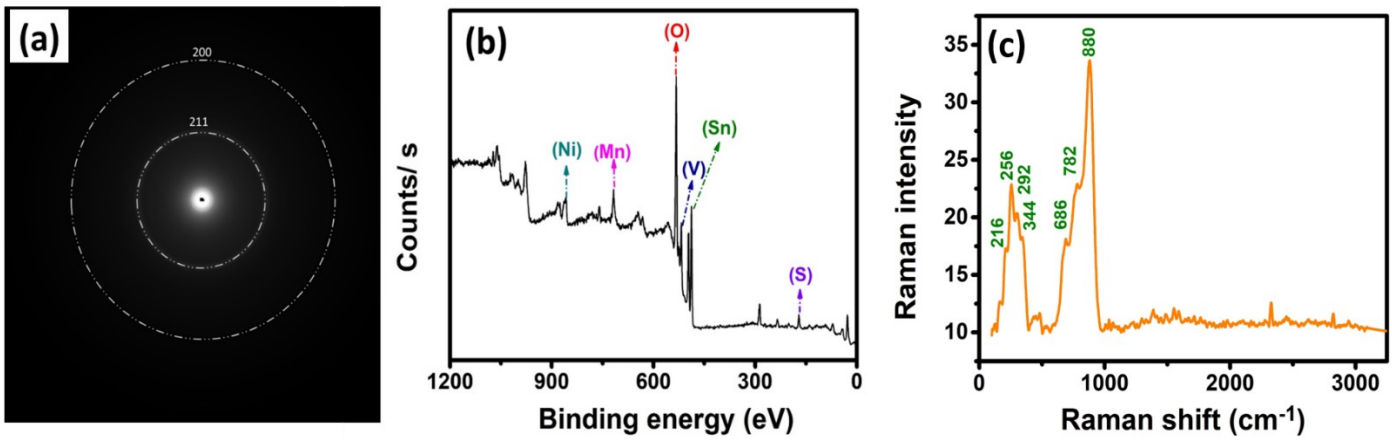

Figure S1. (a) SAED pattern of as-fabricated composite, represent 211 and 200 crystal plans of metallic tin, (b) XPS survey spectrum, and (c) Raman spectrum for the as-prepared composite.

Table S1. Atomic ratios based on XPS analysis.

Element	Ni	Mn	O	V	Sn	S
Atomic ratio %	45.34	29.9	11.39	6.77	2.77	3.85

Synthesis of heretical nitrogen-doped carbon (HDC)

Using disodium EDTA as a carbon-nitrogen precursor ($C_{10}H_{14}N_2Na_2O_8$) in a direct pyrolysis method produce carbon doped nitrogen with hieratical structure. The thermally treatment was carried out under Argon gas flow in a ceramic boat into a horizontal thermo-scientific tube furnace at 800 ºC for 2 hours, with a ramping rate 5 ºC.min^{-1} for both heating and cooling processes. Then, the obtained black residue product was firstly washed by diluted HCl followed by deionized water washing until pH 7. Finally, the sample was filtrated carefully, then dried overnight at 80 ºC. The produced heretical nitrogen-doped carbons here are denoted as HDC.

Morphology of HDC was investigated using SEM as shown in Figure S1a and b, where reveals an interconnected channel would provide fast electrolyte diffusion and rapid charge transfer upon the use of such materials in energy storage devices. The XRD patterns of the HDC material displays in Figure S1c, which exhibited (002) and (100) diffraction peaks related to the stacking of graphene interlayers and ordered graphene domains, respectively. Furthermore, the surface analysis of HDC studied using the nitrogen adsorption/desorption isotherms as Figure S2a. The isotherms exhibited a sharp increase of the nitrogen sorption at low pressure ($P/P_o < 0.2$), revealing the existence of micropores. Also, the observed hysteresis loop at a high relative pressure ($P/P_o > 0.3$) revealed the presence of mesopores [48]. Based on the IUPAC classification, all samples exhibit type–IV sorption isotherm with h4-type hysteresis loops. thus, the thermal treatment led to the successful formation of bimodal micro/mesoporous nitrogen doped carbons with high surface area of 1424 m.g^{-1} and average pore volume of 0.78 cm^3.g^{-1}. Additionally, the desorption BJH pore size distribution plots shown in Figure S2b confirm the coexistence of microporous and mesoporous structures of ~1.6 and ~3 nm, respectively. The combined

micro/mesoporous structure is expected to facilitate the movement of ions during the charge process and pot it as a good relevant of negative electrode.

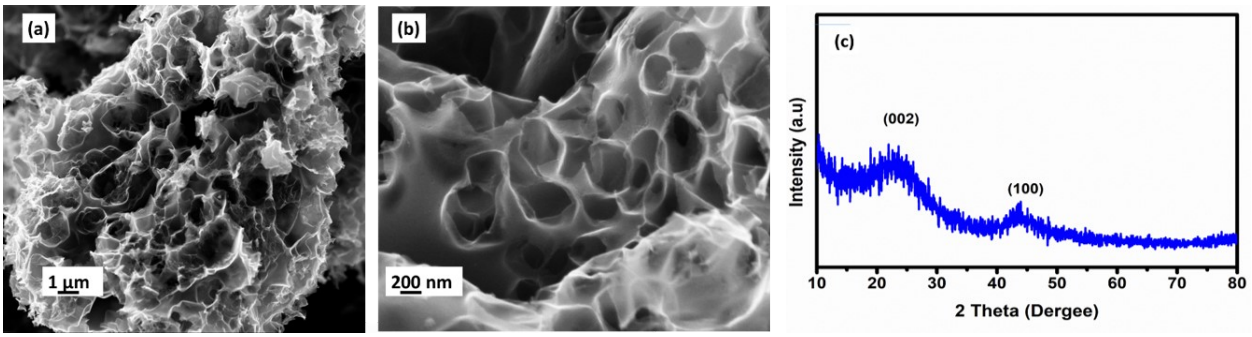

Figure S2. (a and b) SEM at high and low magnification and c XRD pattern of the HDC.

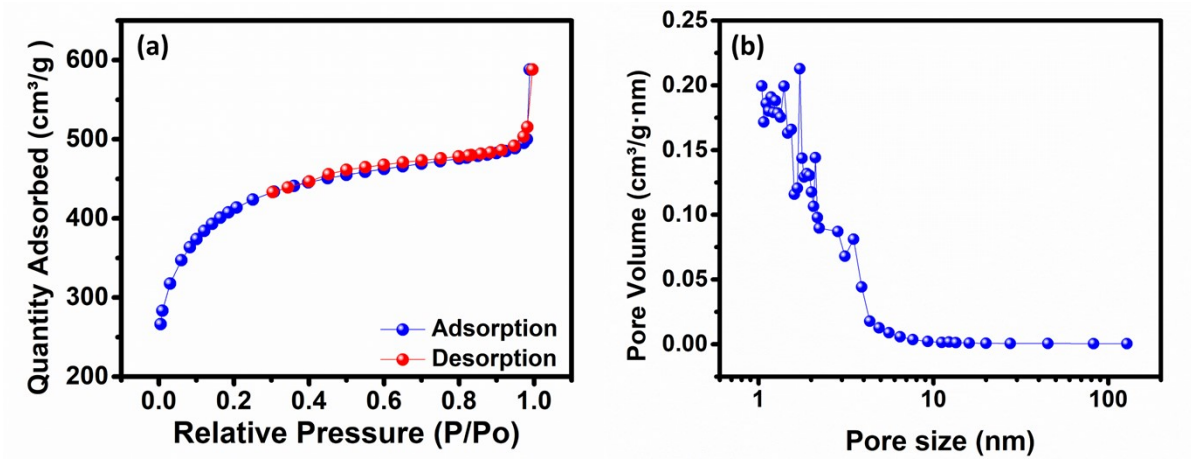

Figure S3. The N_2 adsorption/desorption isotherms And d) BJH pore size distribution of the HDC.

To investigate HDC as negative electrode, a three electrode measurements were carried out using 1 M KOH, with electrode loaded mass of ~ 1 mg. Figure S3a represent CV of HDC at different scan rates and achieved a high capacitance of 569 $F.g^{-1}$ with high rate capability of 53% at 50 $mV.s^{-1}$. Moreover, the CED at different current densities of HDC displays in Figure S 3b and d with pseudo behavior. Additionally, the Nyquist plot in Figure S2c displayed a small semicircle with linear Warburg indicating the good diffusion and by using Z-fit, the charge transfer resistance

was found to be 0.52 Ohm. Worth mention that the HDC sustain the same behavior at high scan rates and current densities owing to the high surface are and low charge transfer.

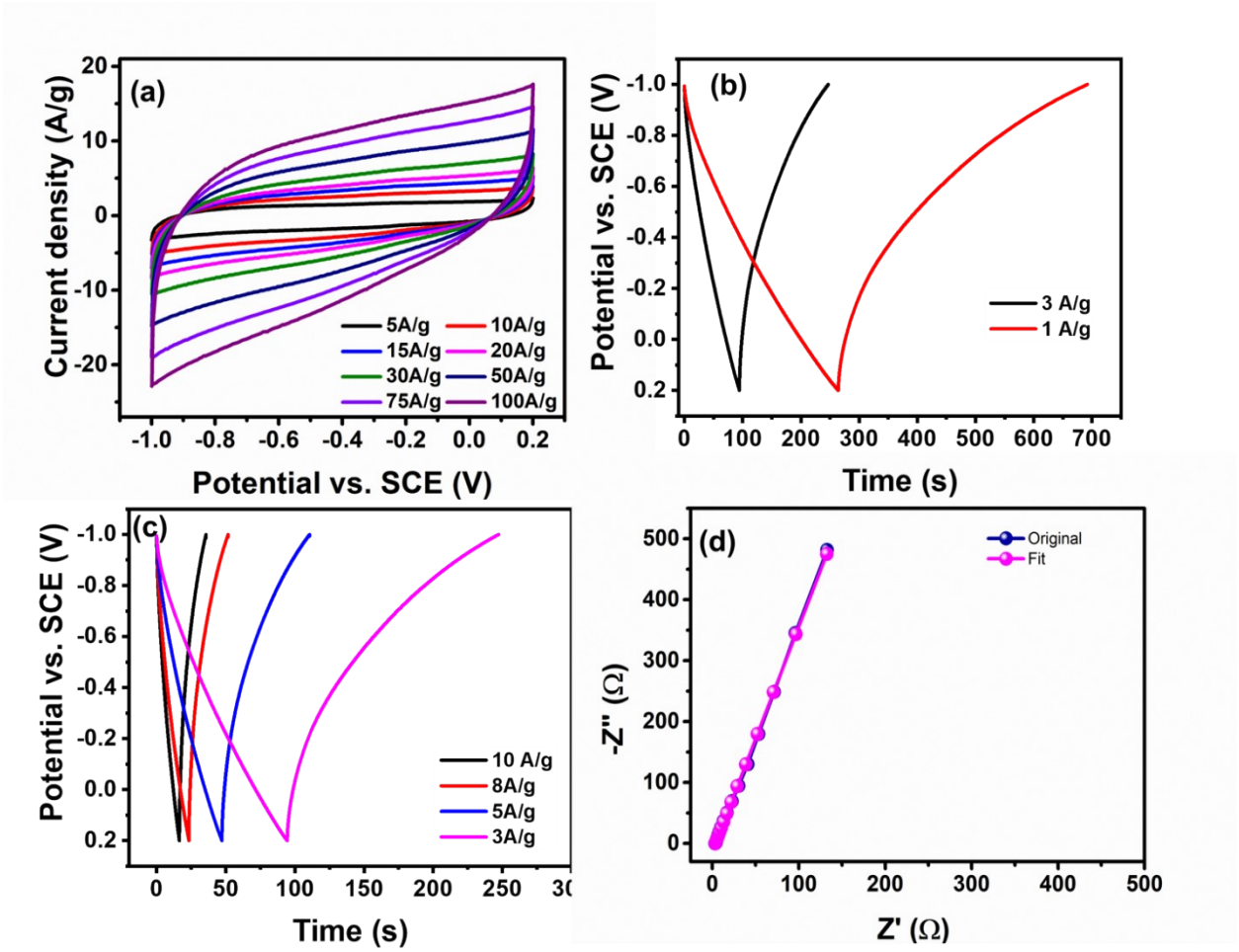

Figure S4. a) CV, b and c) CED and d) Nyquist plot of HDC as negative electrode.

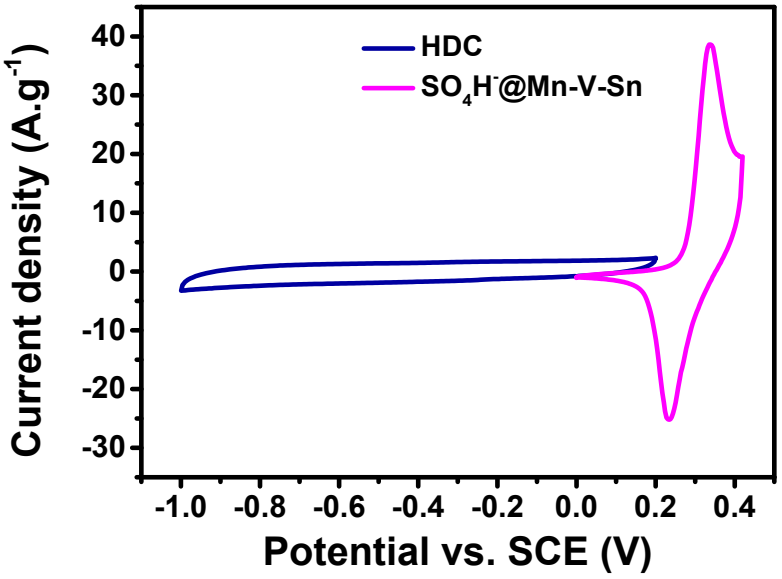

Figure S5. CV profiles of Negative and positive poles at 5 mV.s^{-1} .

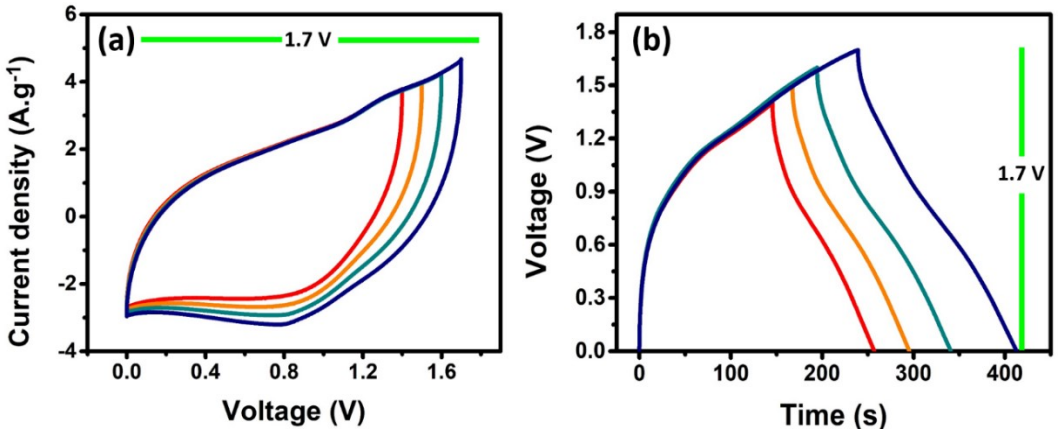

Figure S6. Device operating in different potential windows from (1.4-1.7 V), (a) CV at 20 mV.s^{-1}, (b) CED at 1.5 A.g^{-1}.

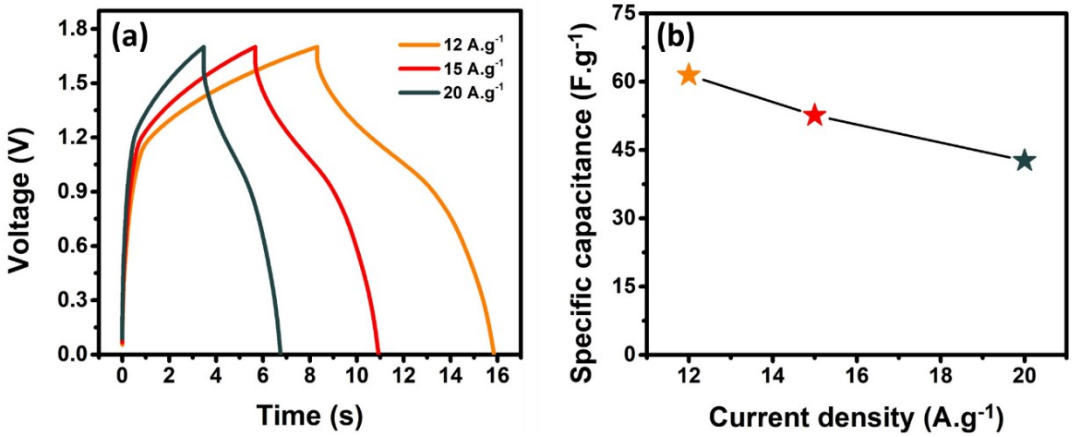

Figure S7. (a) CED curves, (b) Specific capacitance as a function of current density. At current different densities from 12-20 $A.g^{-1}$.

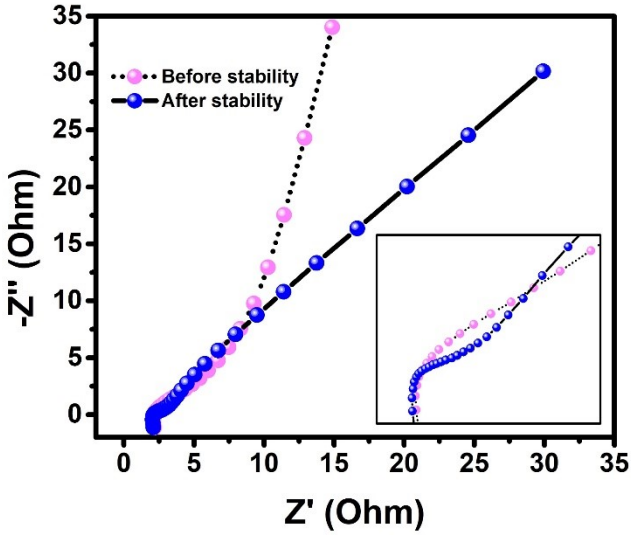

Figure S8. Nyquist plot for two electrode system before and after stability measurements.